



HAL
open science

Impact of humidification by cathode exhaust gases recirculation on a PEMFC system for automotive applications

S. Rodosik, J.-P. Poirot-Crouvezier, Y. Bultel

► **To cite this version:**

S. Rodosik, J.-P. Poirot-Crouvezier, Y. Bultel. Impact of humidification by cathode exhaust gases recirculation on a PEMFC system for automotive applications. *International Journal of Hydrogen Energy*, 2019, 44 (25), pp.12802-12817. 10.1016/j.ijhydene.2018.11.139 . hal-02337129

HAL Id: hal-02337129

<https://hal.science/hal-02337129>

Submitted on 22 Oct 2021

HAL is a multi-disciplinary open access archive for the deposit and dissemination of scientific research documents, whether they are published or not. The documents may come from teaching and research institutions in France or abroad, or from public or private research centers.

L'archive ouverte pluridisciplinaire **HAL**, est destinée au dépôt et à la diffusion de documents scientifiques de niveau recherche, publiés ou non, émanant des établissements d'enseignement et de recherche français ou étrangers, des laboratoires publics ou privés.



Distributed under a Creative Commons Attribution - NonCommercial 4.0 International License

Impact of humidification by cathode exhaust gases recirculation on a PEMFC system for automotive applications

S. Rodosik^{1,2,3*}, J.-P. Poirot-Crouvezier¹ and Y. Bultel^{2,3}

¹*Univ. Grenoble Alpes, CEA, LITEN, DEHT, F-38000 Grenoble, France*

²*Univ. Grenoble Alpes, LEPMI, F-38000 Grenoble, France*

³*CNRS, LEPMI, F-38000 Grenoble, France,*

Corresponding author. Univ. Grenoble Alpes, CEA, LITEN, DEHT, F-38000 Grenoble, France.

E-mail address: sandrine.rodosik@cea.fr (S. Rodosik), jean-philippe.poirot@cea.fr (J.-P. Poirot-Crouvezier), yann.bultel@grenoble-inp.fr (Y. Bultel).

Abstract:

Reactant gases humidification, in most PEM fuel cell systems, is traditionally implemented to ensure both stack durability and superior performance. A cathode exhaust gases recirculation architecture allows to decrease the system volume compared to the passive humidifiers, which are classically used. Incorrect water management being responsible for irreversible degradations, a control of relative humidity at stack inlet thanks to the recirculation could be of a great interest to limit their impact. In this work, investigations on performance and stability are performed during operation in recirculation mode, from the cell scale to the system scale. It was observed that high to medium recirculation ratio were able to stabilize and homogenize the cells voltages along the stack but performance was reduced due to oxygen dilution by nitrogen. Besides, large relative humidity ranges were achieved at stack inlet, which can vary from 25 to 85% and could be able to follow automotive dynamics.

Keywords:

Cathode exhaust gases recirculation

Fuel cell system

Gases humidification

Water management

Proton exchange membrane fuel cell

Transport applications

1. Introduction

With the growing interest in the hydrogen economy, Proton Exchange Membrane Fuel Cells are promising components for systems dedicated to transport applications. Indeed, their low operating temperature and high energy density make them suitable for the automotive industry. However, these systems are still facing several challenges on their way to mass market production. Reaching a durability of 5000 h recommended by the U.S. Department of Energy and decreasing system cost are major hurdles to their development.

Gases humidification in PEMFC systems is necessary to ensure best performance as well as long-term stability. It allows establishing a proper water management that is to say, operate with stable conditions avoiding cell flooding and drying in the stack, and favor a longer lifetime. Despite its large volume and thermal inertia, the most used technology at the cathode side is a passive humidification technique, called in this study “classic humidification”. This technology allows transport to the cathode inlet of water collected at the cathode exhaust, thanks to selective mass transfer through hollow fiber membranes. It can be classified among “external humidification solutions”, where humidification of the gaseous reactant flow is realized before the fuel cell inlet. Even though fuel cell durability is strongly dependent on water management [1–3], relative humidity control with such component is hardly feasible without affecting the operating conditions and stack voltage. Many other external humidification solutions have been developed, including liquid water transport through membranes, bubblers, enthalpy wheels, or direct water injection, in liquid or vapor form. The latter offers a possibility to control the water amount injected at the cathode inlet whereas passive techniques are completely dependent on the fuel cell operating conditions. In some cases, no external humidification solution is used in fuel cell systems, which is designated as “internal humidification solutions”. These latter consist in self-humidification of the fuel cell, where the reactant flows are humidified directly inside the fuel cell by the water produced by the electrochemical reaction. They can be improved by modifications of the cell components material composition in either the MEA or the gas diffusion layer or the cell design, more specifically channel design [4] [5]. Self-humidification can also be achieved by special operating control strategies such as low temperature operation or high pressure [6] [7] focusing on water transport through the fuel cell membrane.

Several external and internal humidification solutions have been studied in literature. Büchi and Srinivasan [8] tested a single cell of 50cm² active area during 1800h with an internal humidification solution, i.e. fed with dry hydrogen and air. They observed 20 to 40% performance losses compared to an external humidification solution enabling the injection of gases saturated with water vapor. Besides, they noticed that the maximum temperature to establish a stable behavior of the fuel cell with the self-humidification mode was 70°C.

Otherwise, the cell tended to dry out. They also concluded that diffusion of water through the membrane was sufficient to ensure water management in a wide range of operating conditions. Recently, Martin et al. [9] tested several Pt loading electrodes prepared by the electro spraying deposition technique. These cells were dedicated to self-humidification operation. They achieved long-term operation but at a maximum temperature of 60°C and obtained low performance: 600mV at 0.2A/cm². Hwang and Kim [10] studied the coupled effect of humidification and cooling using direct liquid water injection inside the fuel cell. The experiments were held at high current densities with a 5-cells PEMFC stack with 250 cm² MEA. They concluded that the method was more efficient for cell humidification at the lowest temperature (i.e. 60°C) and obtained better performance than with an external humidification system enabling an inlet relative humidity (RH) of 60%. Migliardini et al [11] studied three different external humidification solutions at the cathode including bubblers, heat and mass exchange by selective polymeric membranes and active humidification by water injection. They compared it with an internal humidification solution. In their study, self-humidified fuel cells were considered as the best solution for automotive applications, with high control possibilities but at a maximum cell temperature of 55°C. Sanchez et al [12] studied the performance and stability of the cell voltage with temperature and relative humidity variations. They compared voltage responses at 60°C and 80°C on a single cell of 142cm². At equivalent relative humidity levels (50/50 at both sides), they recorded a voltage improvement of 4.8% at 80°C. However, decreasing cathode RH to 20% was sensitive and caused a drying behavior at higher temperature due to a flowrate higher at the cathode than at the anode. Indeed, the voltage response could drop of 21%. They noticed that drying could be compensated by a sursaturated flow at the anode side and recorded a voltage drop of only 8%. They finally recommended to operate at very high relative humidity at the anode when the humidification at the cathode is inferior to 50%. Iranzo et al. [13] performed a parametric study on a 50-cm² cell including RH, current density and air stoichiometric ratio variations and concluded that cathode RH had a stronger influence on the cell performance than anode RH. Neyerlin [14] studied the Oxygen Reduction Reaction kinetics under low relative humidity and concluded that a minimum RH level around 50-60% was necessary for the ORR to occur independently from RH values.

All of these studies show that water management with either internal or external humidification solutions is complex. An accurate humidification can be achieved with self-humidification in variable conditions but only at low temperature, whereas external humidifiers allow to achieve better cell performance at high temperature. Nevertheless, the latter are not suitable to ensure best water management following power variations, such as automotive conditions, because of their slow dynamic. Besides, low temperature operation

lead to a higher cooling subsystem sizing. As automotive system volume tend to be reduced in order to ease their integration, operation temperature should be increased. Removing cathode external humidifiers from the system is highly desirable in the objective of decreasing the system mass and volume. However, in order to prevent membrane dehydration, we suggest a system composed of a recirculation loop at the cathode side. This architecture is called the Cathode Exhaust Gases Recirculation (CEGR) or cathodic recirculation. CEGR appears as a suitable solution to humidify air at the cathode side using water vapor produced by the fuel cell. Besides, cathodic recirculation has the advantage to modulate the relative humidity at stack inlet by varying the amount of water recirculated from the stack outlet. It can be considered as an active water management solution since the humid gas flow mixed with fresh air before the stack inlet is controlled with a compressor speed. In contrast, during operation with passive humidifiers, relative humidity at stack inlet is mainly imposed by operating pressure, temperature and stoichiometric ratio ("Sto").

Various recirculation architectures have been patented in recent years, as in [15–21]. However in literature only few studies deals with CEGR[22–30]. To our knowledge, Yang et al. [22] were the first to study a new stack architecture allowing humidification at the both sides of the membrane with reactant recirculation. They worked with three cascaded cells. Therefore, the cells are connected in series, each of them humidifying the next one. A recirculation loop at both anode and cathode allows to humidify the first cell from the last one. Their study was mainly focusing on start-up at 30°C, 1 bar. They concluded that the cathode recirculation had more effect than the anode one. Moreover, they noticed that cathode flooding could be avoided thanks to the recirculation. More recent work from Kim and Kim [23] introduced the recirculation ratio defined as the ratio of the molar recirculated gas flow on the total gaseous flow at the cathode outlet. They suggested two different architectures of CEGR to remove external humidifiers. The first one included only one compressor for the mix of fresh and recirculated air. The second architecture had two compressors, one for fresh air compression and the second one for the recirculated flow. They only modeled the first architecture and used simulation results to obtain the cathode gas inlet composition and carry out performance experiments on a 5-cells stack. They observed a voltage drop around 7% at 1.0 A/cm² with a low recirculation ratio. They also compared the effect of oxygen dilution and relative humidity at stack inlet on the cell voltage, and observed that the first one had a higher impact. Unfortunately, no experiment was performed with high recirculation. On the same architectures, Junming et al. [24] modeled only one system with a single compressor similarly to Kim and Kim [23] and proposed a control strategy for water management with cathode EGR. Cheng [25] was interested in oxygen dilution by recirculation for voltage clamping, while Jiang et al [26] and Xu et al. [27]

studied recirculation at both sides of the membrane. All of them concluded that recirculation could achieve the same relative humidity levels as external humidifiers, but that voltage could be reduced due to the oxygen dilution at the cathode inlet. This can be an advantage in startup or idle states, because it could avoid degradations occurring at voltage levels higher than 0.8V. However, all of these studies have been conducted at very low current and high stoichiometric ratios.

To our knowledge, very few experimental works have been performed with multi-scale analysis. On a real-scale system equipped with CEGR architecture, we focused on the system efficiency as well as the stack performance, and the different cells behaviors through the stack thanks to in-line electrochemical impedance spectroscopy. Some experimental studies have been performed on real-scale systems by Kim et al. [31] on a 80-kW system, or Wahdame et al. [32] on a 5-kW system but both were only focused on stack and system performance. In our study, a 5 kW-system built for operation representative of automotive conditions has been used: pressure below 1.5 bar and temperature above 65°C. In this work, the system was equipped with a 70-cells stack. We studied the impact of CEGR under various current densities, temperatures, pressures, stoichiometric ratios and recirculation ratios, and a comparison with passive humidification was done. A design of experiments has been performed and analyzed to look for optimum operating conditions and evaluate the interest of cathode exhaust gases recirculation.

2 Material and methods

2.1 System and stack architecture description

The fuel cell stack used in this work is a 70-cells stack. Commercial MEAs with active area 220cm² have been assembled with serpentine design bipolar plates. More details about cell design have been developed in previous work [33]. Table 1 presents the system specifications.

Table 1: System characteristics

Parameter	Value
MEA	Commercial
Cell number	2×35
Max power	5 kW
Operating temperature	60 to 70°C
Operating pressure	1.2 to 1.5 bar
Maximum fresh air flow	20 Nm ³ /h

Compression ratio in recirculation line	1.12
Ping-Pong frequency	0.9 Hz
Interval between purges at anode	50 s

The studied system presented in Figure 1 is composed of two specific architectures. At the cathode side is implemented the CEGR. It is a recirculation architecture similar to the one presented in the work of Min Soo Kim [23] and Jiang [26]. Fresh air is first filtered and compressed by compressor 1 to reach the stack inlet pressure. At the cathode outlet, liquid water is separated from the exhaust gases. A part of the exhaust is reinjected at the stack inlet through the compressor 2 whereas the other part is evacuated. Compressor 2 is designed to compensate the pressure drops in the stack and the phase separator. At the anode side, a particular architecture, developed at CEA LITEN [31,32], is built. It is called “anode alternative feeding”, or more briefly “Ping-Pong”. Its singularities are in the stack conception and in the alternative fuel feed location. The fuel cell stack is divided into two parts with 35 cells each. Various hydrogen circulation configurations are possible, as both half-stacks can be connected in series or in parallel. It can be considered close to Dead End Anode with some modifications to avoid water and nitrogen accumulation in the cells. Operating conditions usually obtained with anode recirculation are achieved without the need of a pump or an ejector. The complete sequence is described in Figure 2. In Figure 2 (a) hydrogen is fed at the left half stack. A solenoid valve opens the left circuit, feeding the left half-stack from its H₂ inlet. All the cells of this half-stack are fed in parallel from their H₂ inlet. Since the outlet manifolds of both half-stacks are connected in the central plate, the right half-stack is fed from its H₂ outlet, and its cells are fed in parallel from their own H₂ outlet. Then in Figure 2 (b), Hydrogen feeds of the right half stack. 1.1 second after the first sequence in (a), the left solenoid valve closes and the right one opens. The same process beginning by the right half-stack arises. Right cells are fed from their inlet and left cells from their outlet. Finally, in Figure 2 (c) is presented the purge sequence. As liquid water and nitrogen accumulate, every 50 seconds, all 3 solenoid valves open to remove efficiently the non-desired species. With purge period set at 50 seconds and purge duration 0.5 second, anode stoichiometric ratio is 1.02 and equal to DEA anode stoichiometric ratio in the same conditions. Figure 2 (d) presents the air feed configuration. The air is fed by the terminal plate close to cell number 70. Then air flows through all cells in parallel and exhaust gases are removed at the same side as the air feed.

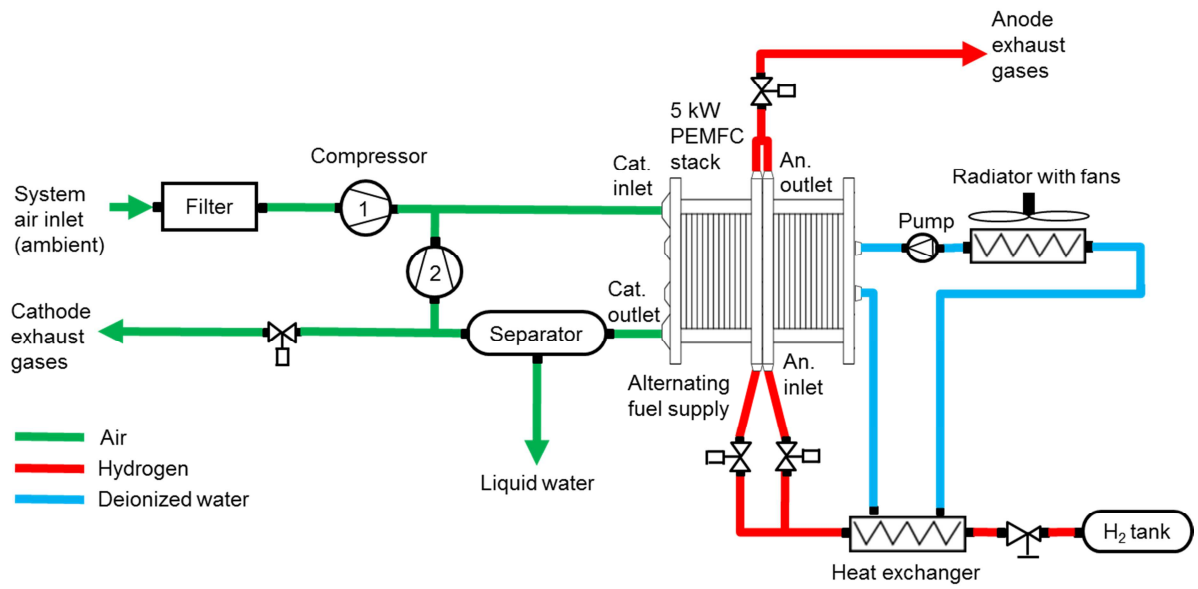


Figure 1: Schematic of the fuel cell system

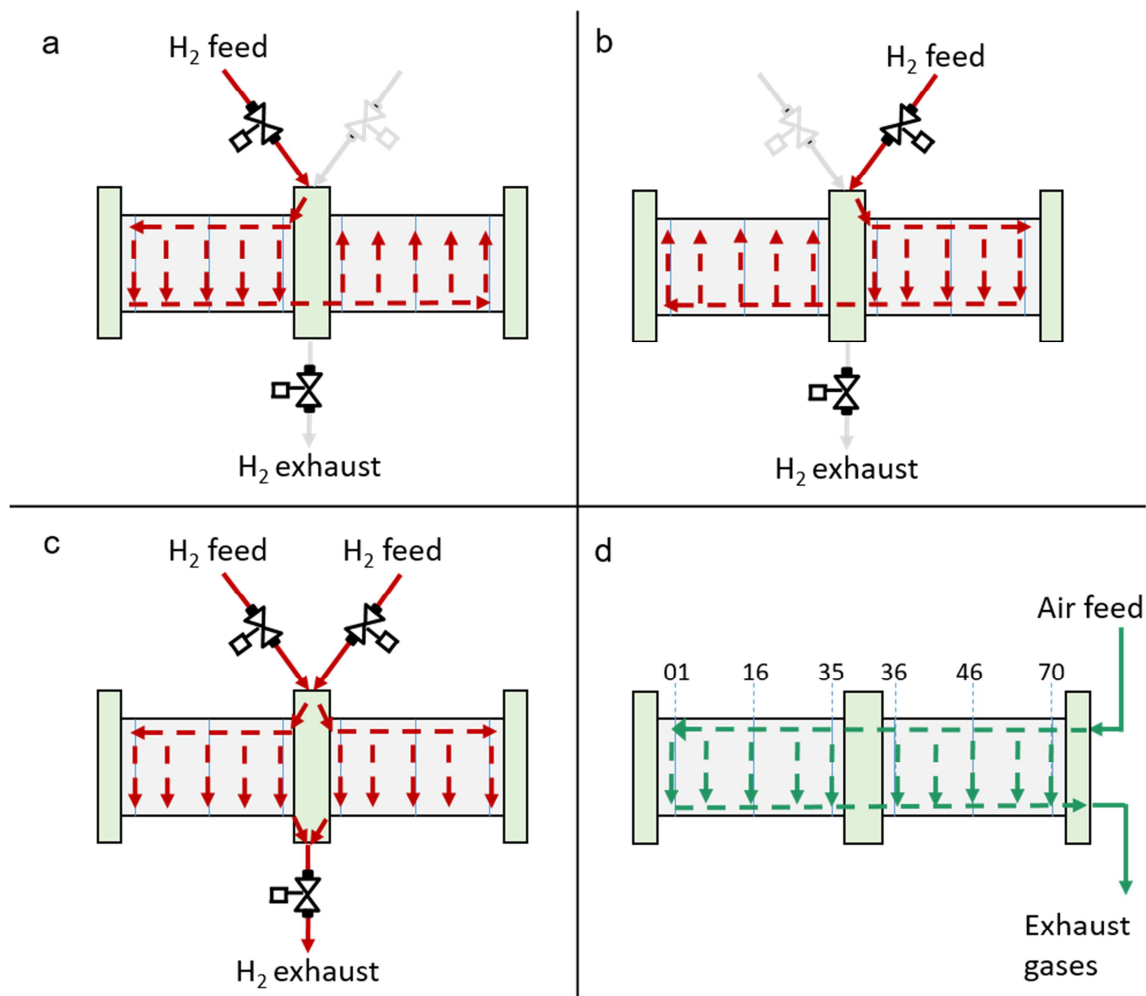


Figure 2: Stack architecture and Ping-Pong strategy, (a) Hydrogen feed of the left half stack, (b) Hydrogen feed of the right half stack, (c) Purge, (d) Air distribution configuration with cell number locations

As no humidifier has been added on the hydrogen line, water transport through the membrane ensures the self-humidification of the anode side, and the Ping-Pong strategy enables homogenization of water vapor along the stack. Liquid water mainly accumulates in the common outlet manifold, acting as a phase separator. Open/close commutation frequency of the two feeding valves is set at 0.9 Hz in this study. This value was identified as the optimum to avoid flooding in individual cells. A complete study of the Ping-Pong strategy and optimization is beyond the scope of this paper and will be performed in further work.

A radiator and fan control on a deionized water-cooled loop ensures thermal management. During operation, stack outlet temperature is maintained stable within $\pm 1^\circ\text{C}$ tolerance. The cooling loop is also used to preheat hydrogen before the anode inlet in a tubular heat-exchanger.

For the purpose of comparison of different humidification solutions at the cathode side, two passive humidifiers FC-150 series, mounted in parallel, from Permapure® (not presented on Figure 1) are also installed on the test bench. They are used when the cathode recirculator is turned off, and by-passed when the recirculation mode is used. Thus, experiments carried out with the passive humidification mode are performed on the same system as recirculation experiments. Therefore, the impact of system components is equivalent and the results with both architectures can be compared.

2.2 Full factorial design of experiment

In order to deeply study the effect of cathodic recirculation on the PEMFC behavior, a complete Design of Experiments (DoE) has been built including 5 parameters. The current density, pressure (similar at anode and cathode), stack temperature, air stoichiometry as well as the recirculation ratio were identified as variables. For each one, three levels (low, medium and high) are investigated. All parameters and DoE levels are gathered in Table 2. The limitations of the test bench in terms of fresh air flow and pressure, mentioned in Table 1, restricted their variation range.

In order to decrease system volume, automotive systems tend to increase temperature to decrease the radiator sizing. That is the reason why a temperature of 70°C was chosen as the maximum level in the DoE. The minimum temperature studied here is 60°C, considering that a lower temperature is not realistic for automotive application. So, the three temperature levels are 60, 65 and 70°C. The pressure range was chosen as large as possible, considering the capabilities of the compressor. Consequently, the three pressure levels were fixed at 1.2, 1.35 and 1.5 bar.

System stoichiometry in recirculation mode was intentionally set lower than with classic humidification since recirculation increases the flowrate at stack inlet. Therefore, to reduce the power consumption of compressor 1, system stoichiometry is set from 1.4 to 1.8 instead of 2 in classic humidification process. A definition of the recirculation ratio "R", similar as Kim and Kim's study [23], was used in the DoE and will be presented in the modelling section: 3.1. Recirculation ratio values could not be similar for the different current densities because of the limitations of the recirculation pump, which are both its maximum flowrate (20 Nm³/h) and its maximum pressure ratio (1.12). For each current density value, the maximum recirculation ratio reachable with the recirculation pump was determined: 0.60 for 0.3 A/cm² and 0.33 for 0.5 A/cm². It was also evaluated equal to 0.16 for a higher current density of 0.7 A/cm². However, it corresponds to a very limited range of recirculation ratio. As a consequence, this current density value was not studied further. Then three levels of recirculation ratio were determined for the remaining current density levels. The low, medium

and high recirculation levels are respectively 0.19, 0.34 and 0.48 at 0.3A/cm² and 0.13, 0.22 and 0.32 at 0.5A/cm². The recirculation flow is limited by the dimensioning of recirculation components, and more precisely of the recirculation pump. When the recirculation flow increases, the pressure drops inside the air pipes and in the stack also increase. In the present study case, the pressure ratio of the recirculation pump is high enough to obtain recirculation ratios of 0.48 at 0.3 A/cm² and 0.32 at 0.5A/cm².

Table 2: Design of Experiment parameters and levels used for recirculation characterization

DoE values	Lower level	Medium level	Higher level
Current density	0.3 A/cm ²	0.5 A/cm ²	-
Temperature	60°C	65 °C	70°C
Pressure	1.2 bar	1.35 bar	1.5 bar
Stoichiometry	1.4	1.6	1.8
Recirculation ratio	low	Medium	high

The DoE gathered 162 operating points, which were performed randomly for each temperature value since thermal steady state was long to establish. At start-up, the test bench steady state was considered to have been reached after operating 40 minutes at fixed operating conditions. Between each operating point, steady state was considered to have been reached after 15 minutes. In every case, the measurement was recorded during 800 seconds after stabilization.

3 Modelling of cathode exhaust gases recirculation

3.1 CEGR model description

In order to be able to predict the relative humidity at stack inlet for any operating conditions and demonstrate the benefits of the use of cathodic recirculation in a system, a simplified model based on mass balances was built. The model uses the following assumptions:

- Calculations on the gas phase is performed assuming ideal gas equations
- Phase separators remove 100% of liquid water (or separator yield is 1)
- Temperature is assumed constant in all components, except in compressors, and is equal to stack temperature
- Gas and water transports through the fuel cell membrane are neglected
- The system exhaust flow rate is saturated of water vapor

To be able to control the recirculated flow, a new variable has to be defined as the recirculation ratio “R”. This variable is defined as the ratio of the recirculated molar flow N^{rec} on the gaseous stack outlet molar flow $N^{sep,o}$ (only considering gas flow) to obtain a value ranging from 0 to 1:

$$R = \frac{N^{rec}}{N^{sep,o}} \quad (1)$$

Assuming no gas transport through the membrane, nitrogen is conserved during operation at the cathode side. Introducing the system stoichiometric ratio Sto^{sy} , using the Faraday’s law, and the usual molar fraction for the air composition, the nitrogen flow at the system outlet $N_{N_2}^{sy,o}$ is:

$$N_{N_2}^{sy,o} = N_{N_2}^a = \frac{n_{cell} \cdot I \cdot Sto^{sy} \cdot 0.79}{4F \cdot 0.21} \quad (2)$$

Where $N_{N_2}^a$ is the nitrogen molar flow at the system inlet coming from the ambient air, n_{cell} the number of cells in the stack, I the current and F the Faraday constant.

Similarly, the oxygen flow in the exhaust gases $N_{O_2}^{sy,o}$ can be defined using Faraday’s law for oxygen consumption:

$$N_{O_2}^{sy,o} = N_{O_2}^a - N_{O_2}^c = \frac{n_{cell} \cdot I}{4F} (Sto^{sy} - 1) \quad (3)$$

As water condensation occurs at the stack outlet, the gaseous mix at the system outlet is saturated. And so, the water molar fraction at the system outlet $x_{H_2O}^{sy,o}$ can be expressed thanks to the saturation pressure at stack temperature $P_{sat}(T^{st})$ and the total pressure $P^{sep,o}$ at the phase separator outlet:

$$x_{H_2O}^{sy,o} = \frac{P_{sat}(T^{st})}{p^{sep,o}} \quad (4)$$

Then, the gaseous flow $N_{gas}^{sep,o}$ can be written thanks to a combination of equation (1) to (4):

$$N_{gas}^{sep,o} = \frac{N_{O_2}^{sy,o} + N_{N_2}^{sy,o}}{1 - x_{H_2O}^{sy,o}} \cdot \frac{1}{1 - R} \quad (5)$$

At the cathode inlet, the molar flow rate of each specie i (oxygen and nitrogen) is expressed as:

$$N_i^{c,i} = N_i^{sy,i} + R \cdot N_i^{sep,o} = N_i^{sy,i} + \frac{R}{1 - R} \cdot N_i^{sy,o} \quad (6)$$

Where $N_i^{sy,i}$ is the molar flow rate of specie i at the system inlet and $N_i^{sy,o}$ the molar flow in the exhaust gases.

Using Faraday’s law for oxygen consumption and using the stoichiometric ratio at the system inlet Sto^{sy} , the equation (6) becomes for oxygen:

$$N_{O_2}^{c,i} = \frac{n_{cell} \cdot I}{4F} \left(Sto^{sy} \left(1 + \frac{R}{1 - R} \right) - \frac{R}{1 - R} \right) \quad (7)$$

The stoichiometric ratio at the system inlet is a value classically used to control the air flow at the stack inlet. However, in our case the air flow at the system inlet is different from the stack inlet because of the recirculation. Consequently, a new definition of the stoichiometric ratio at stack inlet Sto^{st} is defined as follows:

$$Sto^{st} = Sto^{sy} \left(1 + \frac{R}{1-R}\right) - \frac{R}{1-R} \quad (8)$$

This definition shows that when recirculation is set at maximum namely $R=1$, $Sto^{st} \rightarrow +\infty$ and when $R=0$ i.e. without recirculation, $Sto^{st} = Sto^{sy}$.

The amount of water vapor reinjected at stack inlet may be expressed based on the equation (6) and a balance at the phase separator. In constant operation, all the water produced is rejected at the system outlet, either with the other gases in vapor form or in liquid form at the phase separator. Thus, the molar fraction of water $x_{H_2O}^{c,i}$ at the cathode inlet can be written independently from the water production rate but from the recirculation ratio, saturation pressure at stack temperature (in $x_{H_2O}^{sy,o}$) and operating parameters:

$$x_{H_2O}^{c,i} = \frac{x_{H_2O}^a \cdot N_{tot}^a + R \cdot x_{H_2O}^{sy,o} \cdot N^{sep,o}}{N_{tot}^{c,i}} = \frac{x_{H_2O}^a (1 + x_{H_2O}^a) + \frac{R}{1-R} x_{H_2O}^{sy,o} \frac{(4.76 Sto^{sy} - 1)}{1 - x_{H_2O}^{sy,o}}}{\frac{Sto^{sy}}{0.21} (1 + x_{H_2O}^a) + \frac{R}{1-R} \frac{(4.76 Sto^{sy} - 1)}{1 - x_{H_2O}^{sy,o}}} \quad (9)$$

The relative humidity at the stack inlet is then simply derived from the water fraction at stack inlet:

$$RH^{c,i}(T^{st}) = \frac{x_{H_2O}^{c,i} \cdot P^{c,i}}{P_{sat}(T^{st})} * 100 \quad (10)$$

Finally, considering the balance of all species and with similar development to the equation (9), the oxygen molar fraction at stack inlet can be given by:

$$x_{O_2}^{c,i} = \frac{\left(\frac{1 - x_{H_2O}^a}{4.76}\right) Sto^{sy} + \frac{R}{1-R} (Sto^{sy} - 1)}{\frac{Sto^{sy}}{0.21} (1 + x_{H_2O}^a) + \frac{R}{1-R} \frac{(4.76 Sto^{sy} - 1)}{1 - x_{H_2O}^{sy,o}}} \quad (11)$$

3.2 Model results and validation

The expressions developed in the model show that water and oxygen content are dependent on the recirculation ratio and operating conditions but independent from the consumption/production rate.

The Figure 3 (a) shows the decrease of the oxygen molar fraction at the stack inlet with the increase of both the recirculation ratio and the stoichiometric ratio at the system inlet. It is worth mentioning that the consumption of oxygen during operation induces a decrease of the

oxygen molar fraction at stack outlet, while nitrogen, which is an inert specie in the process, dilutes the other species. Therefore, at stack inlet, a higher system stoichiometric ratio increases the oxygen molar fraction, whereas a higher recirculation ratio decreases drastically the oxygen molar fraction. For example, the latter can drop down to 12.2%mol at $Sto^{sy}=1.4$ and 0.8 recirculation ratio. Therefore, oxygen starvation effect might occur with high recirculation ratio impacting the stack performance.

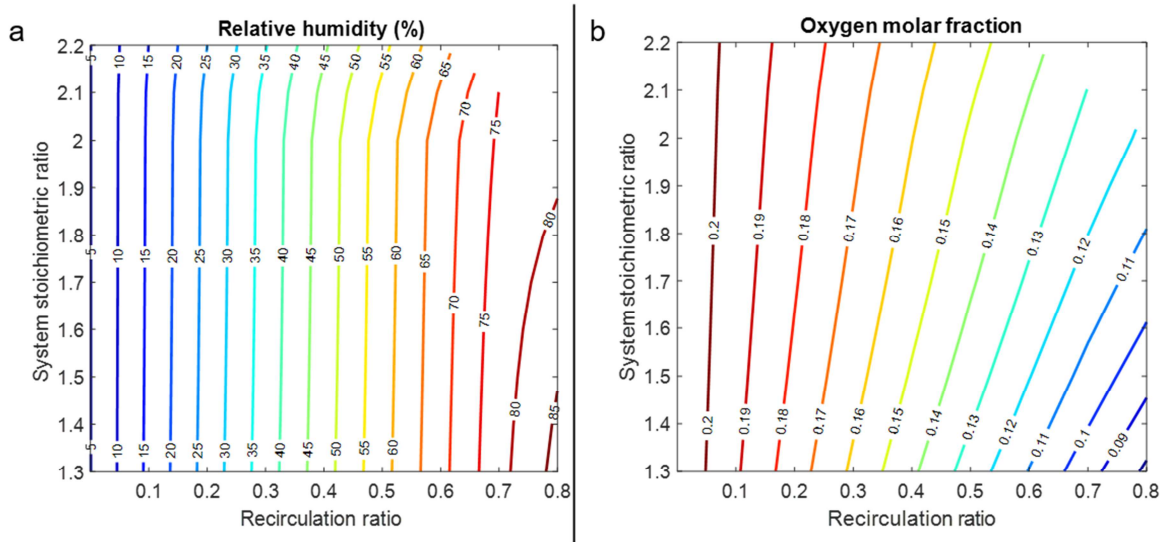


Figure 3: Simulation with constant parameters 0.3A/cm², 1.35 bar, 65°C and air feed at ambient temperature (20°C, 40% RH, Patm) (a) Oxygen molar fraction variations at stack inlet and (b) Relative humidity variations at stack inlet with recirculation ratio and system stoichiometric ratio.

The Figure 3 (b) presents the simulated relative humidity levels reached with increasing recirculation and system stoichiometric ratio. It is observed that a relative humidity higher than 50% can be achieved with recirculation ratio higher than 0.4. According to the model results, a wide relative humidity range could be achieved varying the recirculation ratio (R). For instance, at fixed $Sto^{sy} = 1.8$, relative humidity could be set between 10 and 80% with R varying from 0.05 to 0.8. The Figure 4 shows the simulated RH at two different current densities (i.e. 0.3A/cm² and 0.5A/cm²), varying the recirculation ratio (R). In both cases, a very good agreement is observed between the model and experimental data obtained on the range of recirculation ratio feasible with the test bench. We can notice a gap at high recirculation ratio probably due to the pressure drops in the recirculation line, for which the accuracy of the model at high recirculation ratio can be discussed. Additionally, according to the model, no condensation is supposed to occur when mixing the recirculated flow with the fresh compressed air. Indeed, the fresh air at the system inlet being heated through the compressor 1, its temperature is close to the stack temperature. So, mixing both flows at similar temperature levels is achieved without liquid water formation. Relative humidity at stack inlet is thus only dependent on the amount of water recirculated in the gaseous phase.

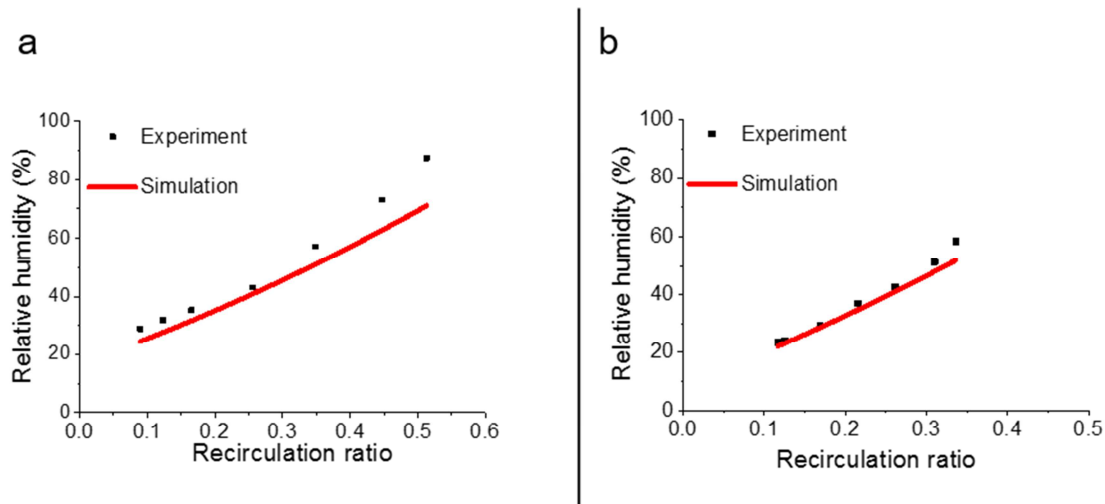


Figure 4: Model validation of the relative humidity levels reached with recirculation ratio variations at operating conditions: 1.5 bar, 60°C, $Sto^{sy}=1.8$, (a) 0.3 A/cm², (b) 0.5 A/cm²

The relative humidity range available with recirculation ratio control is very interesting compared to the passive humidification possibilities. In the examples presented in the Figure 4, variation range can reach 60% at 0.3A/cm² and 38% at 0.5A/cm² respectively. The RH range is reduced when the current density increases due to the limitations of the recirculation device in terms of flow and pressure ratio. With passive humidifiers, variations of the relative humidity can only be hardly established by varying all the operating conditions of the stack. For instance, when using our test bench with passive humidification in standard conditions (1.2 bar, 60°C, 0.3A/cm², $Sto=2$), the relative humidity is around 85%. The lowest relative humidity achievable is about 35% and may be reached with a by-pass of one of the two humidifiers and an increase of the stack temperature from 60°C up to 80°C. The latter temperature increase may reduce the cell durability.

4 Experimental result analysis and discussion

4.1 Impact of the operation conditions on the stack performance

This section investigates the influence of the operating conditions on the stack performance with CEGR mode to compare it with passive humidification. Temperature, pressure as well as system stoichiometric ratio may have an impact on the stack performance.

The Figure 5 presents the influence of temperature, pressure and system stoichiometric ratio, on the cell voltage averaged over the stack and the measurement period for the three recirculation levels selected in the DoE definition. Regardless of the recirculation ratio, the stack performance decrease when increasing the stack temperature. Moreover, Figure 5 (a,b) highlights a severe voltage drop at 70°C at a minimum recirculation level. Indeed, the

recirculation at a minimum level induces a lower relative humidity at stack inlet. This behavior is more pronounced at higher temperature, where the drying process is reinforced. The Figure 5 (a) shows an increase of the stack performance at a current density of 0.3 A/cm² when increasing R. It is different in Figure 5 (b), with a current density of 0.5 A/cm², where the cell voltage seems independent from the R level at 60 and 65°C. These low variations could be explained by the recirculator sizing since recirculation ratio range at 0.5A/cm² is quite small. However, performance at 70°C drastically drops for both current density cases and is even unstable at very low recirculation ratio (a stable voltage point cannot be obtained at 0.5A/cm²). At this higher temperature, the minimum relative humidity drops to 20% at 0.3 A/cm² for low R and is even lower at 0.5A/cm². Increasing the recirculation ratio to the maximum, the relative humidity reached at 0.3A/cm² is around 50% but only 30% at 0.5A/cm². So, water amount is not sufficient to obtain a correct hydration level of the membrane whatever the R value at 0.5 A/cm² and high temperature (i.e. 70°C). A higher recirculation ratio would be necessary to bring a higher water content with the aim of stabilizing the voltage at higher temperature. This is consistent with existing data in literature at low RH values [14], [34].

The Figure 5 (c) and (d) show the positive impact of a pressure increase on stack voltage, respectively at 0.3 A/cm² and 0.5 A/cm². At 0.3A/cm², the low pressure case meets the optimum conditions at medium recirculation ratio. However, at higher pressure, the increase of oxygen partial pressure seems to slightly move the optimum to higher recirculation ratios than the one measured. At 0.5A/cm², the voltage increases with the recirculation ratio at low pressure, when the partial pressure of water is low. On the contrary, with higher pressure, the recirculation level seems to have no effect due to the increase of water partial pressure, reducing the drying effect.

Finally, Figure 5 (e) and (f) present the influence of the system stoichiometric ratio on stack voltage, respectively at 0.3 A/cm² and 0.5 A/cm². Maximum performance is observed at $Sto^{sy}=1.8$ at 0.3A/cm² and $Sto^{sy}=1.6$ at 0.5A/cm². In additions, optimum performance is obtained at medium recirculation ratio at $Sto^{sy}=1.8$ for both current densities and $Sto^{sy}=1.6$ at 0.5A/cm². The existence of an optimum behavior will be analyzed in part 4.2. Indeed, higher Sto^{sy} might increase stack voltage by increasing the oxygen content at the stack inlet, but also induces a voltage drop due to cell drying (i.e. too much dry air is fed in the total air flowrate at the cathode inlet). The drying effect was effectively observed at high current density (0.5A/cm²) when best performance is obtained at $Sto^{sy}=1.6$. Indeed, in this case, relative humidity was 4% higher than the case at $Sto^{sy}=1.8$. The behavior at $Sto^{sy} 1.6$ and low current density seems to show that the optimum is not reached and would be at a higher recirculation ratio than 0.48. A rise of R can increase the relative humidity at stack inlet, but

will decrease oxygen partial pressure too. Combining both phenomena, we can observe optimum performance with a set of stoichiometric ratio/recirculation ratio.

At low current density, rising the stoichiometric ratio increases the voltage for any recirculation ratio. The optimum voltage of 710 mV is observed at medium recirculation ratio with $Sto^{sy} = 1.8$. It is different at higher current density where, a Sto^{sy} of 1.6 with medium recirculation ratio gives the best performance: 586 mV.

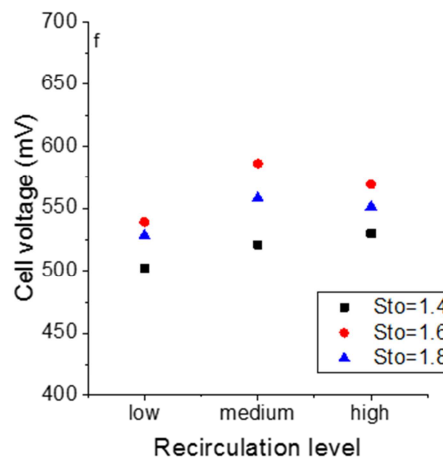
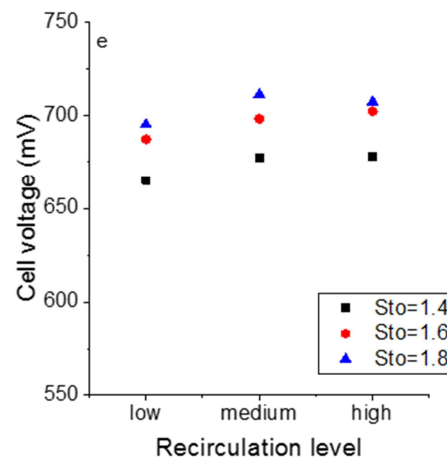
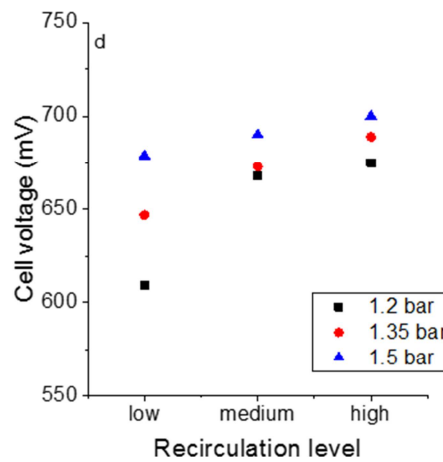
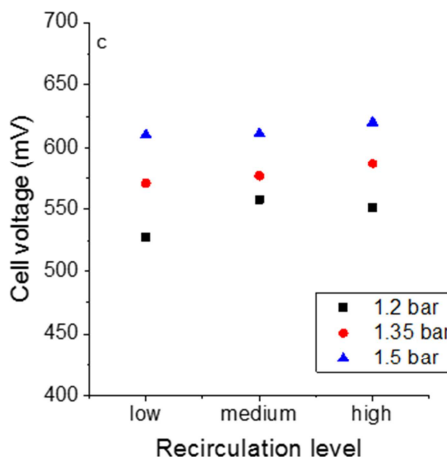
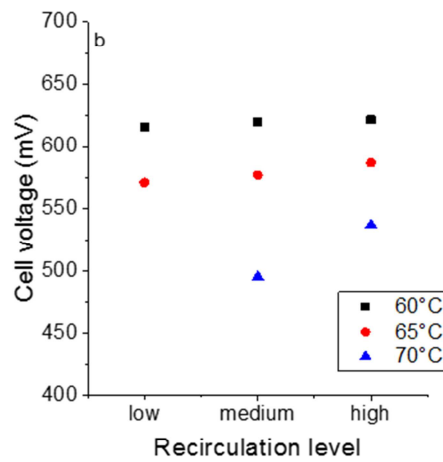
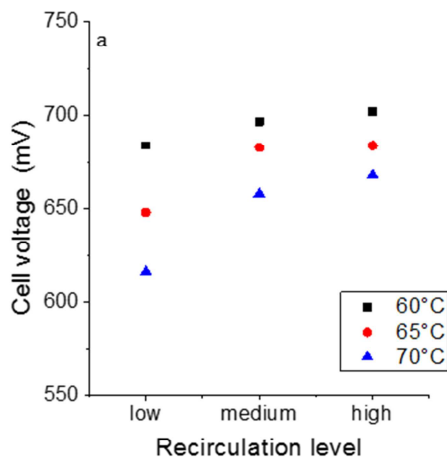


Figure 5. Mean cell voltages obtained with variable recirculation levels: (a) impact of stack temperature at 0.3A/cm², 1.35bar and Sto^{sy}=1.8, (b) impact of stack temperature at 0.5A/cm², 1.35bar and Sto^{sy}=1.8, (c) impact of stack pressure at 0.3A/cm², 70°C and Sto^{sy}=1.8, (d) impact of stack pressure at 0.5A/cm², 65°C and Sto^{sy}=1.8, (e) impact of Sto^{sy} at 0.3A/cm², 1.2 bar and 60°C, (f) impact of Sto^{sy} at 0.5A/cm², 1.2 bar and 65°C

In order to show the limited impact of temperature and pressure on RH with passive humidifiers, several experiments have been performed. The influence of the pressure was first investigated, the other operating parameters remaining constant: 0.5A/cm², 65°C, Sto^{sy}=2. The results showed a relative humidity decrease of 8% with a cell voltage increase from 611 mV to 628 mV when the pressure rises from 1.35 up to 1.5 bar. Secondly, a temperature step of 5°C was imposed, from 65 to 70°C with constant parameters: 0.3A/cm², 1.5 bar, Sto=2. Similarly, a low relative humidity decrease of 4% has been recorded with a 3mV voltage loss, namely from 703 mV to 700 mV. These experiments highlight the limitations of water management with passive humidifiers since it is mainly designed for a narrow operating range. It could be enlarged with cathodic recirculation, thanks to RH modulation.

4.2 Impact of recirculation on cell performance around optimum conditions

This second section investigates more deeply the influence of the recirculation ratio on the cell performance for both current densities namely 0.3 and 0.5 A/cm². The Figure 6 illustrates the behavior of mean cell voltage (stack voltage divided by cell number) as well as the lowest cell voltage in the stack and the highest one when increasing the recirculation ratio. All three values are averaged over the measurement period. Three different domains can be distinguished as a function of the recirculation ratio.

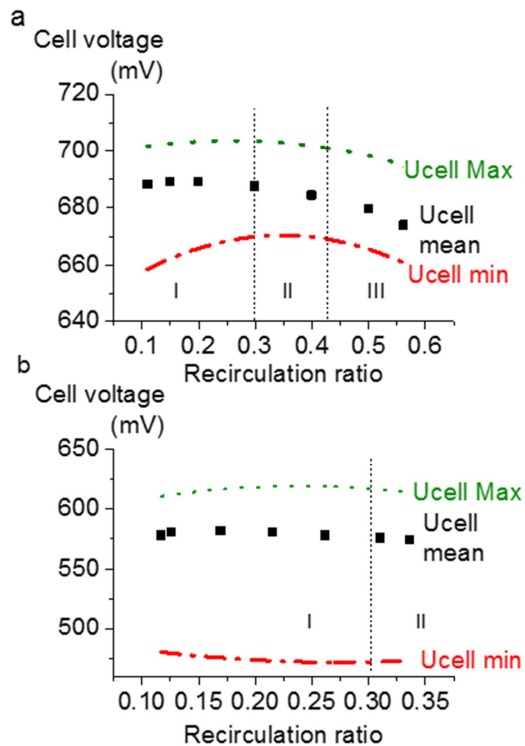


Figure 6: Voltage response of minimum (red dashed line), maximum (green dotted line) and mean (black squares) cells in the stack as a function of the recirculation ratio at 60°C ; 1.5 bar ; system stoichiometric ratio = 1.8, (a) 0.3 A/cm², (b) 0.5 A/cm²

At very low recirculation levels referred to as zone I in Figure 6 (a) and (b), performance is at its maximum level. However, the gap between the mean and lowest cell voltage value is also maximum, while the difference between mean and highest value is low. This indicates that decreasing recirculation ratio increases cell voltage heterogeneity in the stack. The high difference between lowest and mean voltage, contrasting with the low difference between highest and mean voltage, confirms the hypothesis of cells drying or flooding. However, flooding occurs usually with high relative humidity levels. This latter behavior is probably due to cells drying, because the relative humidity at stack inlet is below 43% at 0.3A/cm² and 51% at 0.5A/cm² when R is lower than 0.3. Some cells located near the air inlet, and potentially subject to a higher air flow than the average, are suspected to be dried.

At moderate or high recirculation rates, the cell voltages are more uniform while the mean cell voltage follows a decreasing tendency. In zone II with recirculation levels between 0.3 and 0.4, as shown in Figure 6 (a), higher stack homogeneity is achieved at 0.3 A/cm². The homogeneity is confirmed by the reduced cell voltage difference between the highest and the lowest value, and the central position of the mean value inside this voltage range. The voltage level is likely comparable to the previous case at low recirculation ratio because of oxygen dilution at the stack inlet. The corresponding relative humidity values are consistent

with the cells behavior. Namely, RH was measured at 43% at $R=0.3$ and RH was recorded at 57% at $R=0.4$. The same behavior can be observed in Figure 6 (b) with the same recirculation ratios. However, the profile is shortened due to the recirculation compressor limitations. The beginning of zone II can be identified from $R=0.3$ while the gap between the maximum and minimum cell voltages is reduced and mean cell voltage start to decrease.

At higher recirculation levels in zone III as referred in Figure 6 (a), the mean cell voltage drop is more visible (-0.5% to -2%) due to the reduction of oxygen partial pressure (see Figure 3). Nevertheless, relative humidity values are still increased with R from 57% to 87% at $R=0.4$ to 0.57 respectively. It appears that stack homogeneity is similar to the previous recirculation zone. It can be concluded that CEGR ensures an efficient cells humidification in zones II and III.

At low current density, namely $0.3\text{A}/\text{cm}^2$, optimum conditions highlighted through the DoE are reached at 60°C , 1.5 bar and $\text{Sto}^{\text{sy}} = 1.8$. The experiments performed at various recirculation ratios show that maximum performance is observed at $R=0.2$, which appears to be a good compromise. With lower recirculation ratio, the decrease of the relative humidity lowers the performance. With higher recirculation ratio, a performance decrease is observed due to oxygen depletion. However, a better homogeneity among the cells is obtained with a higher recirculation ratio around 0.3. Indeed, higher stack stoichiometric ratio and relative humidity resulting from a higher R favor a higher cells homogeneity. That is why we choose to operate with a slight performance loss at a recirculation ratio close to 0.3 in these conditions.

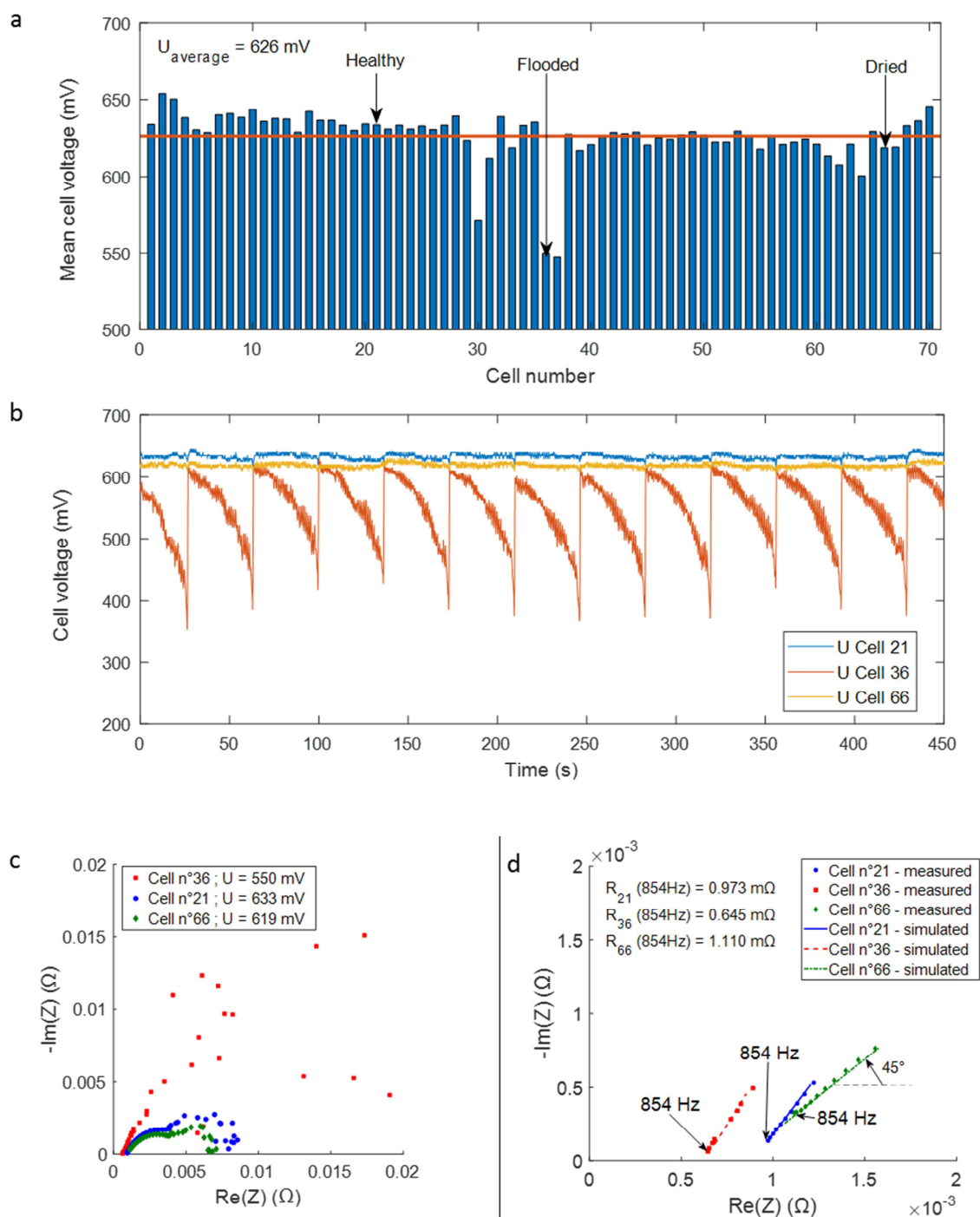


Figure 7: Stack and cell behaviors in dry conditions at 0.3A/cm², 65°C, 1.35 bar, system stoichiometric ratio = 1.8 and recirculation ratio = 0.17 with (a) cell voltage profile along the stack during experiment, (b) Cell voltage temporal measurement for cells 21, 36 and 66 (c) Electrochemical Impedance Spectra of 3 particular cells in the stack : cells 21 healthy, 36 flooded and 66 dried (d) Parameters evaluated from impedance spectra at high frequency : resistance measured at 854 Hz and 45° branch for the dry cell

Further investigations can be observed in Figure 7 for a specific test at low recirculation ratio (zone I) where both dried and flooded cells can be detected. The operating conditions of the test can be considered as dry conditions, with a low recirculation ratio of 0.17, a high system stoichiometric ratio of 1.8, medium temperature and pressure of 65°C and 1.35 bar respectively, and a low current density of 0.3 A/cm². The relative humidity at stack inlet is only 22% in this conditions. The mean cell voltage, averaged over the complete experiment, is 626 mV. Figure 7 (a) shows the cell voltage profile along the stack with mean cell voltages recorded during the experiment. Three particular cell behaviors were compared, corresponding to three different locations inside the stack: close to the air inlet, where cell drying is often observed in dry conditions (cell n°66), between the two half-stacks on the central distribution plate (cell n°36) and in the middle of the other half-stack (cell n°21). Accordingly, the cell voltage versus time profile of these three cells are presented in the Figure 7 (b). Cell number 21 is considered healthy since its mean voltage (633 mV) is higher than the mean cell voltage of the experiment (626 mV). Its location is not impacted by the stack architecture, as it is neither close to the air or hydrogen inlets, nor close to a terminal plate or central plate, where side effects might occur (refer to Figure 2 for flow feed locations). Even if the cell number 21 seems to be healthy, cells number 36 and 66 might be considered as flooded and dried because of their low cell voltage and location in the stack. Cell number 36 is considered flooded because its voltage profile during measurement was periodically rising after each anode purge. As one of the main function of the purge is liquid water removal, it can be anticipated that anode flooding occurs in this cell. The cell number 66, for which the cell voltage is 14 mV lower than the healthy cell, is assumed dried, considering its location near the air manifold inlet, with relatively dry operating conditions. It has to be noticed that thermal side effects have an influence on the cell voltage behavior. Voltages recorded for cells number 68 to 70 are higher than cell 66. Their temperature maybe colder than cell 66 that can explain a lower drying effect.

To confirm these hypotheses, Electrochemical Impedance Spectra have been performed. The frequency ranged between 5000 and 0.1 Hz with 10 points per decade by using a single sine signal in galvanostatic mode (66 A with 10% amplitude). Figure 7 (c) shows the EIS spectra obtained for cells 21, 36 and 66 with their respective mean voltages obtained in the measurement conditions. On the EIS spectra, low frequency loop may be distorted due to the system instabilities. Ping-Pong alternating feed frequency as well as anode purges generate pressure and relative humidity instabilities which can have an impact on the cell behavior. Therefore, only the high frequencies are used for this analysis. So, high frequency resistance measured at 854 Hz characterizing the membrane resistance [35,36] are compared in the Figure 7 (d). For the healthy cell 21, the high frequency resistance

measured at 854 Hz is 0.973 mΩ. For the flooded cell 36, the high frequency resistance measured at 0.645 mΩ confirms this behavior since the value is lower than the healthy cell. As the membrane conductivity is improved with a good hydration level, the resistance is reduced with a higher water content. Therefore, a low resistance value coupled to a low and unstable voltage profile points out a flooding behavior.

For the cell number 66, the high frequency resistance is measured at 1.1 mΩ which is 0.138 mΩ higher than the healthy cell and the typical 45° branch, which looks like a Warburg impedance in the high frequency region for dry spectrum, hints a drying behavior.

These analyses highlight the heterogeneous cell voltage behaviors occurring at low recirculation ratio (in zone I in Figure 6). As relative humidity at stack inlet is reduced, some cells may suffer from drying. Additionally, as the flowrate at cathode inlet is reduced, some particular cells can suffer from flooding.

4.3 Impact of recirculation on stack performance at 70°C

The Figure 8 presents two polarization curves measured with both architectures: passive humidification and recirculation. The common operating conditions for both architectures were set at the same values: temperature at 70°C, pressure at 1.2 bar. These conditions were determined considering automotive conditions. In order to maximize system efficiency, pressure has to be lowered to avoid the energy loss due to the compressor efficiency. Temperature should also be higher to minimize the radiator size.

In order to obtain a stack stoichiometric ratio close to a value of 2 for both cases, a system stoichiometric ratio of 1.8 was imposed for the recirculation mode, with high recirculation ratio. The highest recirculation ratio was also chosen to reach a relative humidity level as high as possible for the complete polarization curve since RH level achieved with classic humidification was close to 85% in this case. The first polarization curve was recorded with classic humidification mode using the passive humidifiers. The second one was recorded with CEGR as humidification solution. An impact of the recirculation process on the fuel cell performance is observed, leading to a small stack voltage loss. During polarization curves, all parameters have to be kept stable, and the speed of the compressor 2 was set to maintain a maximum recirculation ratio for each current density value ranging from R=0.7 to 0.33.

At 70 A ($i=0.32\text{A}/\text{cm}^2$), we observed a voltage difference of 50 mV. This gap is partly explained by the oxygen dilution and by the reduced relative humidity achieved at 70°C. As highlighted in the Figure 3, oxygen partial pressure is reduced due to dilution with recirculation: $x_{O_2}^{c,i dry}=0.15$.

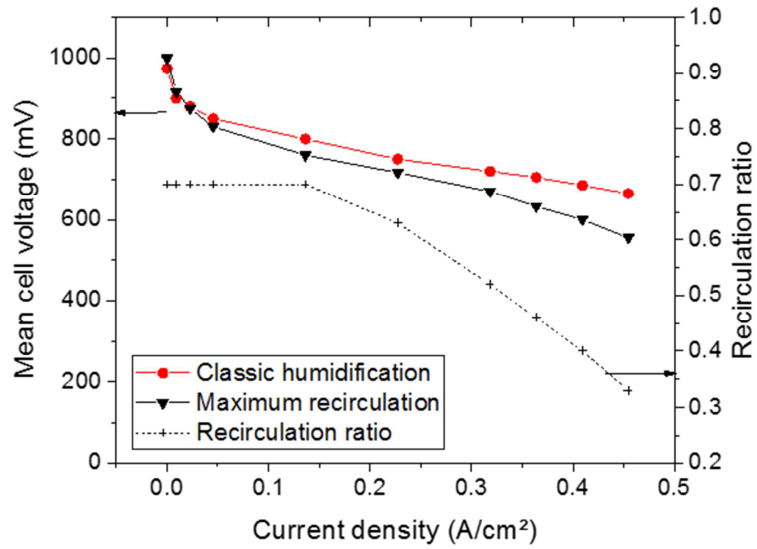


Figure 8: Polarization curves for classic humidification (black triangles) and maximum recirculation (red circles), operating conditions 1.2 bar, 70°C, $Sto^{synt} = 2$ for classic humidification and $Sto^{synt} = 1.8$ for recirculation mode and recirculation ratio variation (dotted line)

4.4 Impact of recirculation on the system performance at 70°C

Performance decrease with recirculation architecture has also an impact on the system efficiency. System efficiency η^{synt} is calculated as follows:

$$\eta^{synt} = \frac{P^{stack} - P^{aux}}{LHV_{H_2} \cdot F_{H_2}} \quad (12)$$

Where P^{stack} is the stack power P^{aux} , the power consumption of ancillaries and LHV_{H_2} the Lower Heating Value of hydrogen and N_{H_2} hydrogen molar flow.

Power consumption of the water pump, solenoid valves or sensors are assumed negligible compared to compressors consumption and so only the latter are considered for calculations ($P_{aux} = P_{comp}$). For sake of simplicity, ideal compressor efficiencies are considered to be free from real component specifications as set in equation (13):

$$P_{comp} = \frac{1.4}{1.4-1} N_{air}^{sy,i} \cdot R \cdot T_a \left(\left(\frac{P^o}{P^a} \right)^{\frac{1.4-1}{1.4}} - 1 \right) \quad (13)$$

Where $N_{air}^{sy,i}$ is the air flow rate at the system inlet in moles, R the perfect gas constant, T_a and P^a the ambient temperature and pressure respectively, P^o the outlet pressure of the compressor.

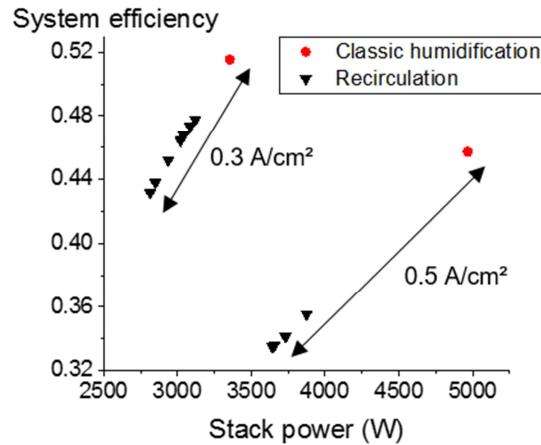


Figure 9: System efficiency with and without recirculation taking into account only compressors as ancillaries for system efficiency calculations. Cell voltage measured at 70°C, 1.2 bar, for classic humidification (red circles) at fixed stoichiometry=2, and for recirculation mode (black triangles) $Sto^{sy} = 1.4$ to 1.8 and variable recirculation ratios

The Figure 9 presents the system efficiencies obtained with both architectures (passive humidification and recirculation) for two different current densities. In the case of CEGR, the recirculation ratio was ranging from 0.19 to 0.48 at the 0.3A/cm² and from 0.13 to 0.32 at 0.5A/cm². As passive humidification experiments have been performed previously for a polarization curve at 70°C and 1.2 bar and $Sto=2$, cell voltage measurements in CEGR mode have been extracted from the DoE at the same temperature and pressure conditions with variable recirculation ratios and stoichiometric ratios to compare their system efficiencies.

A minimum gap of 3.7% on the system efficiency is observed at a current density of 0.3 A/cm² with $R=0.48$ and $Sto^{sy}=1.8$ whereas a larger one of 10.1% is observed at a current density of 0.5 A/cm² with $R=0.32$ and $Sto^{sy}=1.6$. The best performance is obtained with a high recirculation ratio instead of medium because of the operating temperature. The sensitivity analysis in part 4.2 was performed at 60 and 65°C where relative humidity could be slightly lowered without affecting cell performance and stability. In the present case temperature is 70°C, which requires a higher water content at the stack inlet and thus a higher R.

The efficiency difference between passive humidification and recirculation system can be explained with three elements, related to oxygen dilution, relative humidity at stack inlet, and compressor power. First, oxygen dilution at stack inlet induces a voltage drop due to the decrease of oxygen activity in the catalyst layer of the cell. Second, lower inlet gas humidification at the cathode inlet when decreasing the recirculation ratio has a detrimental effect on the stack performance. Finally, theoretical power consumed to compensate stack and air loop pressure drops can represent 4% to 20% of total power consumption for air

compression slightly decreasing the system efficiency. The stack power and system efficiency are therefore lower than the one obtained in passive humidification mode.

To visualize the impact of compression power during operation, the consumption of both compressors is modeled based on the isentropic case written in equation (13) for compressor 1 (fresh air compression). Figure 10 presents the total power consumed by air compression as a function of both the recirculation ratio and the system stoichiometric ratio. It is observed in Figure 10 (a) that ideal recirculation compression is limited compared to fresh air compression and particularly when R is lower than 0.35. Indeed, the compression ratio of the recirculation pump being low compared to the first compressor, the ancillaries power consumption is not very far from the reference case without recirculation. Besides, as Sto^{st} is increased with recirculation, system stoichiometry could be reduced to limit the first compressor consumption and achieve a total power consumption close to the system without recirculation. As an example, a case without recirculation at a Sto^{sy} of 2 has a power consumption equivalent to a recirculation case at $Sto^{sy}=1.75$ and $R=0.5$.

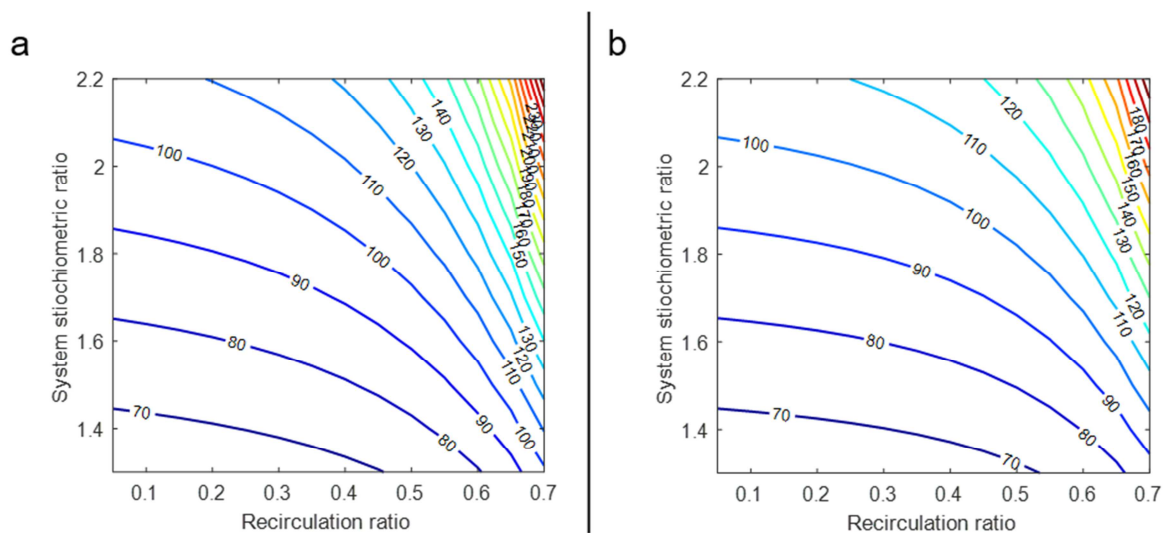


Figure 10 : Theoretical power consumed in Watt by both fresh air compressor and recirculation pump with recirculation ratio and system stoichiometric ratio at the cathode side for a simulated current density at $0.3A/cm^2$, 1.35 bar, $65^\circ C$ (a) normal case based on pressure drops measurements during operation (b) reducing 33% of stack pressure drops

While an increase of the recirculation ratio improves cell voltage stability, it also increases the parasitic power consumed by the recirculation component. One of the main factors influencing this consumption is the value of the pressure drops along the recirculation loop. Therefore, a simulation with reduced stack pressure drops has been implemented to observe the benefits on total power consumption. Figure 10 (b) presents the power consumed with stack pressure drops reduced of a third. It is observed that power consumed is lower than the previous case, the decrease being more pronounced at higher recirculation ratio. For

instance, at $Sto^{sy}=1.8$ and $R=0.6$, the total power consumption is 123W in the first case and 110W in the second case allowing a 10% gain. This highlights the fact that pressure drops in the air loop have to be minimized. The recirculation induces a higher air flowrate at the cathode side and therefore higher pressure drops in the fuel cell. An optimization of the cell design reducing the total stack pressure drops could drastically reduce the power consumption of compressor 2 with a positive impact on the system efficiency.

4.5 Impact of recirculation on the system dynamic

Another advantage of CEGR for integrating in automotive systems compared to classic humidification would be the dynamics. Indeed, relative humidity can be controlled thanks to the recirculation ratio as already presented in part 3.2 and handle large RH ranges. Additionally, CEGR has a faster dynamic than passive humidification. Actually, the water vapor production follows the fuel cell dynamics and is almost immediately recirculated. On the contrary, the dynamic behavior of the passive humidifier is limited by the water transport through the hollow-fiber membranes at its operating temperature and pressure.

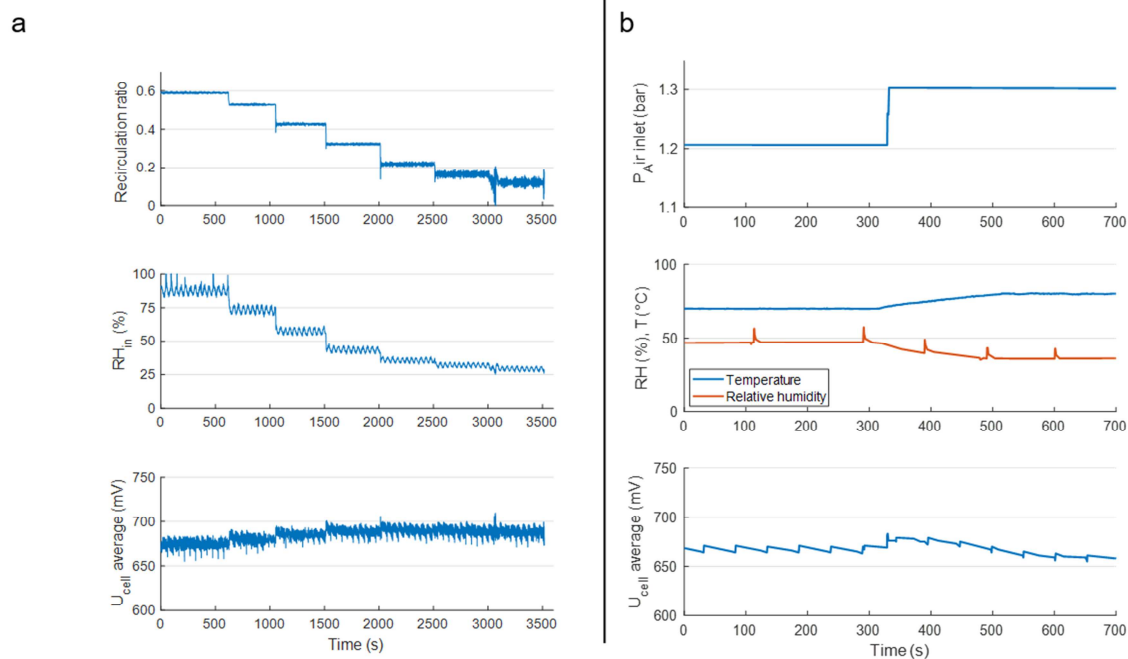


Figure 11: Humidification dynamics comparison between (a) recirculation steps from $R=0.6$ to 0.15 at $0.3A/cm^2$, $1.5bar$, $60^\circ C$ and (b) Passive humidification with a pressure step from 1.2 to 1.3 bar, temperature step from 70 to $80^\circ C$ and $i=0.4A/cm^2$.

The Figure 11 compares the dynamic behavior of the relative humidity with either recirculation or classic humidification. In Figure 11 (a), Recirculation ratio was decreased from 0.6 to 0.15 in several steps with a current density of $0.3A/cm^2$, a temperature at $60^\circ C$ and pressure at 1.5 bar set as constant parameters.

In Figure 11 (b) is presented a temperature increase from 70°C to 80°C and at the same time a pressure variation from 1.2 to 1.3 bar with passive humidification. It is observed in Figure 11 (b) that the temperature reached the set point by a ramp and the relative humidity followed the same trend. Indeed, temperature variations cannot be achieved with steps. On the contrary, as observed in Figure 11 (a), relative humidity can be adjusted instantaneously with recirculation ratio steps.

Besides, with passive humidification, the pressure and temperature changes have a limited effect on relative humidity with a decrease from only 47% to 39%. In contrast, recirculation mode can handle a relative humidity variation from 85 to 26%. The large relative humidity range obtained with recirculation could be a useful tool for water management during fuel cell operation. Indeed, drying could be reduced by recirculation ratio increase to reach relative humidity close to 85%. Additionally, flooding could be avoided by reducing the recirculation ratio.

5. Conclusion

Despite their large volume and thermal inertia, passive humidifiers are classically used in PEMFC systems to humidify the fresh air before the cathode inlet. Besides, their slow dynamic make them not suitable to ensure the best performance following power variations enforced by automotive conditions. In this work, we studied experimentally and theoretically the possibility to reduce the system volume replacing passive humidifiers by a specific architecture at the cathode side, while achieving best performance and stability. This architecture is called the Cathode Exhaust Gases Recirculation (CEGR) and uses the water vapor produced by the fuel cell to humidify the cathode inlet flow. Contrary to passive humidifiers, CEGR offers a possibility to control the water amount injected at the cathode inlet whereas passive techniques are completely dependent on the fuel cell operating conditions. The impact of CEGR was investigated on a 5-kW-system under various current densities (0.3 and 0.5A/cm²), temperatures (60 to 70°C), pressures (1.2 to 1.5 bar), stoichiometric ratios (1.4 to 1.8) and recirculation ratios. It was also compared with performance and stability with passive humidification through a complete Design of Experiment. At first, a simplified model based on mass balances was built in order to predict relative humidity levels at the cathode inlet. The model was validated, and predicts a relative humidity higher than 50% for a recirculation ratio higher than 0.3 and achieve a relative humidity range as large as 60% at 0.3A/cm².

Behavior of the stack under various recirculation ratio conditions was investigated for a fixed temperature, pressure, and system stoichiometric ratio. Three zones were identified as a function of the recirculation ratio value. The first one at low recirculation ratio allows the best

performance but also the worst stability since the water amount is not sufficient to humidify the membrane which started to dry out. In the second zone at medium recirculation ratio, performance is almost equal to the previous one but stability is highly increased. A suitable hydration level was achieved. The third one at high recirculation ratio gives the best stability but performance decrease is higher than in the previous zone (-2%) due to the higher oxygen dilution, even if relative humidity was in a high range. Although performance is lower than with passive humidifiers and current densities higher than $0.5\text{A}/\text{cm}^2$ were not tested due to system components limits, we can recommend using a medium or high recirculation ratio (i.e. zone 2 or 3) for long terms performance and stability for transport applications.

Air humidification thanks to CEGR could also be of great advantage in long-term operation since voltage is reduced by the oxygen dilution. Indeed, carbon corrosion as well as catalyst degradation mechanisms are likely to occur at high cell potential. Decreasing cell voltages when operating at low current may reduce the performance loss and longer the fuel cell lifetime. Durability studies should be performed in order to complete this investigation on the benefits of the architecture.

Acknowledgments

The authors are thankful to Mathieu Giustini, who largely contributed to the experimental work.

References

- [1] Borup R, Meyers J, Pivovar B, Kim YS, Mukundan R, Garland N, et al. Scientific Aspects of Polymer Electrolyte Fuel Cell Durability and Degradation. *Chemical Reviews* 2007;107:3904–51. doi:10.1021/cr050182l.
- [2] Yousfi-Steiner N, Moçotéguy P, Candusso D, Hissel D, Hernandez A, Aslanides A. A review on PEM voltage degradation associated with water management: Impacts, influent factors and characterization. *Journal of Power Sources* 2008;183:260–74. doi:10.1016/j.jpowsour.2008.04.037.
- [3] Pei P, Chen H. Main factors affecting the lifetime of Proton Exchange Membrane fuel cells in vehicle applications: A review. *Applied Energy* 2014;125:60–75. doi:10.1016/j.apenergy.2014.03.048.
- [4] Williams MV, Kunz HR, Fenton JM. Operation of Nafion®-based PEM fuel cells with no external humidification: influence of operating conditions and gas diffusion layers. *Journal of Power Sources* 2004;135:122–34. doi:10.1016/j.jpowsour.2004.04.010.
- [5] Park H. Effect of the hydrophilic and hydrophobic characteristics of the gas diffusion medium on polymer electrolyte fuel cell performance under non-humidification condition. *Energy Conversion and Management* 2014;81:220–30. doi:10.1016/j.enconman.2014.02.029.
- [6] Eckl R, Zehner W, Leu C, Wagner U. Experimental analysis of water management in a self-humidifying polymer electrolyte fuel cell stack. *Journal of Power Sources* 2004;138:137–44. doi:10.1016/j.jpowsour.2004.06.042.
- [7] Zhang J, Tang Y, Song C, Cheng X, Zhang J, Wang H. PEM fuel cells operated at 0% relative humidity in the temperature range of 23–120°C. *Electrochimica Acta* 2007;52:5095–101. doi:10.1016/j.electacta.2007.02.002.

- [8] Büchi FN, Srinivasan S. Operating Proton Exchange Membrane Fuel Cells Without External Humidification of the Reactant Gases Fundamental Aspects. *J Electrochem Soc* 1997;144:2767–72. doi:10.1149/1.1837893.
- [9] Martin S, Garcia-Ybarra PL, Castillo JL. Long-term operation of a proton exchange membrane fuel cell without external humidification. *Applied Energy* 2017;205:1012–20. doi:10.1016/j.apenergy.2017.08.157.
- [10] Hwang SH, Kim MS. An experimental study on the cathode humidification and evaporative cooling of polymer electrolyte membrane fuel cells using direct water injection method at high current densities. *Applied Thermal Engineering* 2016;99:635–44. doi:10.1016/j.applthermaleng.2016.01.091.
- [11] Migliardini F, Unich A, Corbo P. Experimental comparison between external and internal humidification in proton exchange membrane fuel cells for road vehicles. *International Journal of Hydrogen Energy* 2015;40:5916–27. doi:10.1016/j.ijhydene.2015.03.012.
- [12] Sanchez DG, Ruiu T, Friedrich KA, Sanchez-Monreal J, Vera M. Analysis of the Influence of Temperature and Gas Humidity on the Performance Stability of Polymer Electrolyte Membrane Fuel Cells. *J Electrochem Soc* 2016;163:F150–9. doi:10.1149/2.0071603jes.
- [13] Iranzo A, Boillat P, Biesdorf J, Salva A. Investigation of the liquid water distributions in a 50 cm² PEM fuel cell: Effects of reactants relative humidity, current density, and cathode stoichiometry. *Energy* 2015;82:914–21. doi:10.1016/j.energy.2015.01.101.
- [14] Neyerlin KC, Gasteiger HA, Mittelsteadt CK, Jorne J, Gu W. Effect of Relative Humidity on Oxygen Reduction Kinetics in a PEMFC. *J Electrochem Soc* 2005;152:A1073–80. doi:10.1149/1.1897368.
- [15] Knoop A. Apparatus for recirculation of a cathode gas in a fuel cell arrangement, method for shutting down such a fuel cell arrangement. US8691452 B2, 2014.
- [16] Hild T, Herbig T, Wnendt B. Cathode humidification of a PEM fuel cell through exhaust gas recirculation into a positive displacement compressor. US7781084 B2, 2010.
- [17] Goebel SG. Fuel cell shutdown and startup using a cathode recycle loop. US7479337 B2, 2009.
- [18] Garrettson GA, Grupp D, Dabel J. Integrated recirculating fuel cell system. US20120214077 A1, 2012.
- [19] Greszler TA, Robb GM, Salvador JP, Lakshmanan B, Gasteiger H. Shutdown strategy to avoid carbon corrosion due to slow hydrogen/air intrusion rates. US20140038073 A1, 2014.
- [20] Patrick Pelch JW. Système de pile à combustible à recirculation intégrée. WO2016141085A1, n.d.
- [21] Goebel SG. Fuel cell shutdown and startup using a cathode recycle loop. US7691508 B2, 2010.
- [22] Yang T, Shi P, Du C. Study on self-humidified PEMFC with reactant circulation. *Electrochimica Acta* 2006;51:5618–25. doi:10.1016/j.electacta.2006.02.036.
- [23] Kim BJ, Kim MS. Studies on the cathode humidification by exhaust gas recirculation for PEM fuel cell. *International Journal of Hydrogen Energy* 2012;37:4290–9. doi:10.1016/j.ijhydene.2011.11.103.
- [24] Junming H, Liangfei X, Jianqiu L, Ouyang M, Siliang C, Chuan F. Water management in a self-humidifying PEM fuel cell system by exhaust gas recirculation. 2014 IEEE Conference and Expo Transportation Electrification Asia-Pacific (ITEC Asia-Pacific), 2014, p. 1–6. doi:10.1109/ITEC-AP.2014.6941251.
- [25] Cheng S, Li J, Xu L, Ouyang M. Air supply system model with exhaust gas recirculation for improving the life of fuel cell. 2014 IEEE Conference and Expo Transportation Electrification Asia-Pacific (ITEC Asia-Pacific), 2014, p. 1–6. doi:10.1109/ITEC-AP.2014.6941250.
- [26] Jiang H, Xu L, Fang C, Zhao X, Hu Z, Li J, et al. Experimental study on dual recirculation of polymer electrolyte membrane fuel cell. *International Journal of Hydrogen Energy* n.d. doi:10.1016/j.ijhydene.2017.04.183.

- [27] Xu L, Fang C, Hu J, Cheng S, Jianqiu L, Ouyang M, et al. Self-humidification of a proton electrolyte membrane fuel cell system with cathodic exhaust gas recirculation. *Journal of Electrochemical Energy Conversion and Storage* 2017;15. doi:10.1115/1.4038628.
- [28] Jenssen D, Berger O, Krewer U. Improved PEM fuel cell system operation with cascaded stack and ejector-based recirculation. *Applied Energy* 2017;195:324–33. doi:10.1016/j.apenergy.2017.03.002.
- [29] Zhao X, Xu L, Fang C, Jiang H, Li J, Ouyang M. Study on voltage clamping and self-humidification effects of pem fuel cell system with dual recirculation based on orthogonal test method. *International Journal of Hydrogen Energy* 2018. doi:10.1016/j.ijhydene.2018.06.172.
- [30] Alizadeh E, Khorshidian M, Saadat SHM, Rahgoshay SM, Rahimi-Esbo M. The experimental analysis of a dead-end H₂/O₂ PEM fuel cell stack with cascade type design. *International Journal of Hydrogen Energy* 2017;42:11662–72. doi:10.1016/j.ijhydene.2017.03.094.
- [31] Kim DK, Min HE, Kong IM, Lee MK, Lee CH, Kim MS, et al. Parametric study on interaction of blower and back pressure control valve for a 80-kW class PEM fuel cell vehicle. *International Journal of Hydrogen Energy* 2016;41:17595–615. doi:10.1016/j.ijhydene.2016.07.218.
- [32] Wahdame B, Candusso D, François X, Harel F, De Bernardinis A, Kauffmann J-M, et al. Study of a 5 kW PEMFC Using Experimental Design and Statistical Analysis Techniques. *Fuel Cells* 2007;7:47–62. doi:10.1002/face.200500256.
- [33] Nandjou F, Poirot-Crouvezier J-P, Chandesris M, Bultel Y. A pseudo-3D model to investigate heat and water transport in large area PEM fuel cells – Part 1: Model development and validation. *International Journal of Hydrogen Energy* 2016;41:15545–61. doi:10.1016/j.ijhydene.2016.05.117.
- [34] Gößling S, Klages M, Haußmann J, Beckhaus P, Messerschmidt M, Arlt T, et al. Analysis of liquid water formation in polymer electrolyte membrane (PEM) fuel cell flow fields with a dry cathode supply. *Journal of Power Sources* 2016;306:658–65. doi:10.1016/j.jpowsour.2015.12.060.
- [35] Jiujun Zhang, Xiao-Zi Yuan, Chaojie Song, Haijiang Wang. *Electrochemical Impedance Spectroscopy in PEM fuel cells, Fundamentals and applications* n.d. <https://link.springer.com/content/pdf/10.1007%2F978-1-84882-846-9.pdf> (accessed April 23, 2018).
- [36] Springer TE, Zawodzinski TA, Wilson MS, Gottesfeld S. Characterization of Polymer Electrolyte Fuel Cells Using AC Impedance Spectroscopy. *J Electrochem Soc* 1996;143:587–99. doi:10.1149/1.1836485.